Cellular/Molecular

Nanodomain Control of Exocytosis Is Responsible for the Signaling Capability of a Retinal Ribbon Synapse

Tim Jarsky,[1] Miao Tian,[1] and Joshua H. Singer[1,2]

Departments of [1]Ophthalmology and [2]Physiology, Northwestern University Feinberg School of Medicine, Chicago, Illinois 60611

Primary sensory circuits encode both weak and intense stimuli reliably, requiring that their synapses signal over a wide dynamic range. In the retinal circuitry subserving night vision, processes intrinsic to the rod bipolar (RB) cell presynaptic active zone (AZ) permit the RB synapse to encode signals generated by the absorption of single photons as well as by more intense stimuli. In a study using an *in vitro* slice preparation of the mouse retina, we provide evidence that the location of Ca channels with low open probability within nanometers of the release sites is a critical determinant of the physiological behavior of the RB synapse. This gives rise to apparent one-to-one coupling between Ca channel opening and vesicle release, allowing presynaptic potential to be encoded linearly over a wide dynamic range. Further, it permits a transition from univesicular to multivesicular release (MVR) when two Ca channels/AZ open at potentials above the threshold for exocytosis. MVR permits small presynaptic voltage changes to elicit postsynaptic responses larger than quantal synaptic noise.

Introduction

During scotopic (night) vision, the responses of individual rods are propagated to ganglion cells (GCs) by the well-characterized rod bipolar (RB) pathway, as follows: rod → RB → AII amacrine cell → cone bipolar cell → GC (Bloomfield and Dacheux, 2001; Field et al., 2005). Convergence of rod outputs makes individual GCs quite sensitive but presents the RB pathway with two signal-processing problems: (1) separating sparse rod signals from noise at visual threshold; and (2) preventing saturation of the circuitry as light intensity increases by orders of magnitude (Field et al., 2005). Noise reduction is implemented at the rod–RB synapse, and gain is controlled at the RB–AII synapse; amplification follows noise reduction, as is computationally appropriate (Field and Rieke, 2002; Dunn et al., 2006; Dunn and Rieke, 2008). The location of gain control indicates that the intrinsic properties of RB synapses underlie their ability to convey scotopic visual signals over a wide dynamic range.

The coupling between presynaptic Ca influx and the exocytotic machinery exerts a profound influence on the operating range of a synapse. RBs possess ribbon-type active zones (AZs); a near-linear relationship between Ca^{2+} influx and exocytosis has been observed at many ribbon synapses and likely underlies their dynamic range (Thoreson et al., 2004; Brandt et al., 2005; Johnson et al., 2005, 2010; Sterling and Matthews, 2005; Keen and Hudspeth, 2006; Goutman and Glowatzki, 2007). Two cellular mechanisms have been proposed to account for this near linearity: (1) unique Ca^{2+} sensors (otoferlin or non-neuronal synaptotagmins) may initiate exocytosis at ribbon synapses (Thoreson et al., 2004; Dulon et al., 2009; Johnson et al., 2010); and (2) release sites may be controlled by the opening of single Ca channels (the nanodomain control hypothesis) (Brandt et al., 2005; Goutman and Glowatzki, 2007; Li et al., 2009).

Here, we assayed synaptic transmission from RBs to AIIs in a mouse retinal slice preparation to distinguish between these possibilities and to investigate the mechanism(s) responsible for the dynamics of transmission at the RB–AII synapse. First, we determined that exocytosis from RBs is controlled by a conventional vesicular sensor activated by cooperative binding of multiple Ca^{2+} and that release sites are activated by $[Ca^{2+}]$ nanodomains. Second, we found that nanodomain control of exocytosis permitted a transition from univesicular to multivesicular release (MVR) at potentials encountered during RB responses to single photon absorptions. Specifically, physiological stimuli evoked MVR only when presynaptic depolarizations opened multiple Ca channels/AZ; exocytosis evoked by the opening of one channel/AZ was univesicular. Thus, nanodomain control of exocytosis underlies two important properties of the RB pathway: high gain and a wide dynamic range.

Materials and Methods

Tissue preparation. Experiments were performed on slices (200 μm) prepared from light-adapted retinae isolated from wild-type or *Grm6-GFP* C57bl/6 mice of either sex (4–8 weeks old). The *Grm6-GFP* mouse expresses green fluorescent protein (GFP) in all ON bipolar cells, including RBs (Morgan et al., 2006), and was used to target RB terminals for recording. The Animal Care and Use Committee of Northwestern University approved all procedures involving animal use.

Retinae were isolated into bicarbonate buffered Ames medium (Sigma) equilibrated with 95% O_2/5% CO_2 (carbogen) at room temper-

Received March 18, 2010; revised July 8, 2010; accepted July 19, 2010.

This work was supported by National Institutes of Health (NIH) Grant EY-017836, National Science Foundation Grant 0551852, the Alfred P. Sloan Foundation (to J.H.S.) by NIH Grant EY-019828 (T.J.), and by an unrestricted grant from Research to Prevent Blindness to the Department of Ophthalmology at Northwestern University. We thank Drs. W. Grimes, M. Martina, and C. Ratliff for helpful discussion; Drs. E. Mugnaini, L.-G. Wu, and C. Woolley for reading the manuscript; Drs. R. Wong and N. Vardi for the gift of *Grm6-GFP* mice; and P. Chung and V.J. Dudley for technical assistance.

Correspondence should be addressed to Joshua H. Singer, Department of Ophthalmology, Northwestern University Feinberg School of Medicine, 303 E. Chicago Ave., Tarry 5-715, Chicago, IL 60611. E-mail: j-singer@northwestern.edu.

DOI:10.1523/JNEUROSCI.1415-10.2010

 0270-6474/10/3011885-11$15.00/0

ature. For retinal slice preparation, retinae then were embedded in low-melting-temperature agarose (Sigma; type VIIA, 3% in a HEPES-buffered saline), and slices were cut on a vibrating microtome (Microm Corporation). Slices were stored in carbogen-bubbled Ames medium at room temperature until use.

Data collection. All experiments were performed at near-physiological temperature (~34°C). Retinal slices were superfused with a carbogen-bubbled artificial CSF (ACSF) containing the following (in mM): 119 NaCl, 23 $NaHCO_3$, 10 glucose, 1.25 NaH_2PO_4, 2.5 KCl, 2 NaLactate, and 2 NaPyruvate. $CaCl_2$ and $MgCl_2$ were added at varying concentrations to maintain the total divalent cation concentration at 4 mM (e.g., 1 mM $CaCl_2$ and 3 mM $MgCl_2$). Picrotoxin (100 μM); 1,2,5,6-tetrahydropyridin-4-yl) methylphosphinic acid (50 μM); strychnine (0.5 μM); tetrodotoxin (TTX, 500 nM); 2-amino-4-phosphonobutyrate (L-AP4, 2 μM); and niflumic acid (100 μM) were added to the ACSF to block $GABA_A$ receptor-, $GABA_C$ receptor-, glycine receptor-, voltage-gated Na-, mGluR6-regulated, and Ca^{2+}-activated Cl channel-mediated currents, respectively. Drugs were obtained from Sigma or Tocris Bioscience (except for TTX, from Alamone Labs).

Pipettes were filled with the following (in mM): 90 Cs-methanesulfonate, 20 tetraethylammonium-Cl, 1 4-AP, 10 HEPES, 1 BAPTA, 8 Tris-phosphocreatine, 4 Mg-ATP, and 0.4 Na-GTP. Voltage-clamp recordings were made from both RBs and AIIs. Generally, RB holding potential was −60 mV and AII holding potential was −90 mV, and membrane potentials are corrected for junction potentials of approximately −10 mV. Access resistances were <40 MΩ for RBs and <20 MΩ for AII amacrines, and were compensated by 50–90%. Recordings were made using a single MultiClamp 700B amplifier. Synaptic transmission was elicited by stimulation of individual RBs at 10–20 s intervals. Recorded currents and potentials were low pass filtered at 2–8 kHz and digitized at 10–50 kHz by an ITC-18 A/D board (Instrutech) controlled by software written in IGOR Pro (WaveMetrics).

Data analysis. Analysis was performed in Igor Pro and Excel (Microsoft). Recorded Ca currents were leak subtracted offline (P/4 protocol). Paired, two-tailed *t* tests were used to compare paired datasets; ANOVA was used to compare unpaired datasets, and the Mann–Whitney *U* test was used to compare amplitude and rise time distributions. In all cases, significance was accepted as $p < 0.05$. Nonstationary variance analysis was used to estimate single Ca channel conductance. Unless indicated otherwise, data are presented as mean ± SEM, and illustrated traces are averages of 5–10 responses. The traces illustrated in Figure 4*A* and supplemental Figure 3*F* (available at www.jneurosci.org as supplemental material) were digitally filtered at 1 kHz for the purpose of display only.

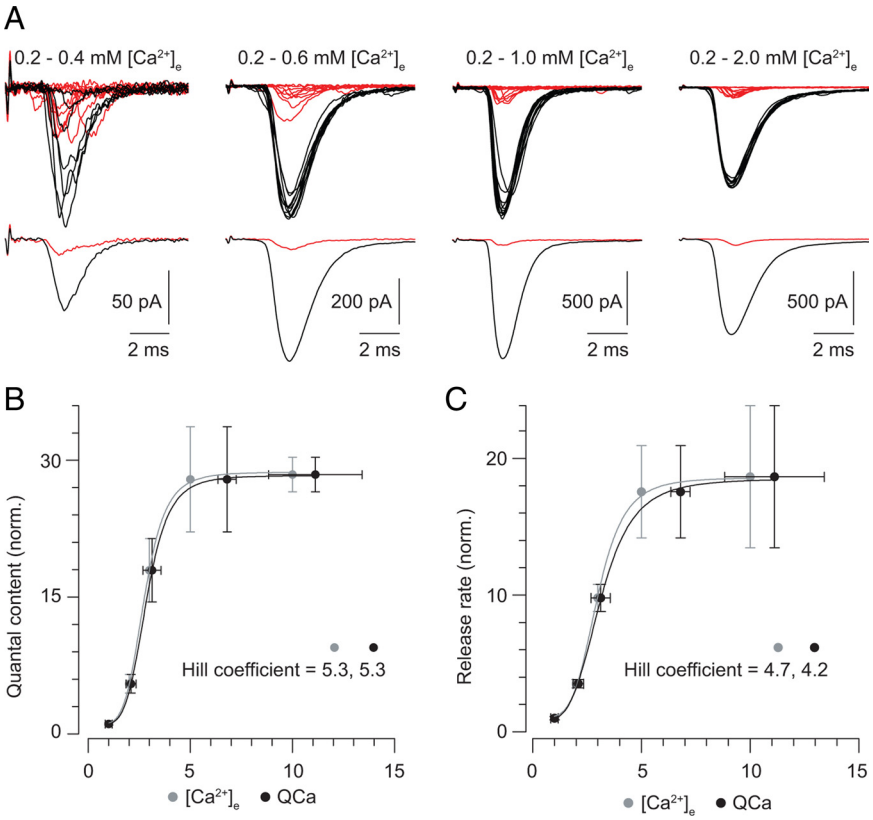

Figure 1. Exocytosis is steeply dependent on $[Ca^{2+}]_e$. ***A***, Representative tail Ca current-evoked EPSCs recorded in 0.2 mM Ca^{2+} (red) and 0.4–2 mM Ca^{2+} (black); each panel illustrates a different paired recording. Note the existence of failures of transmission in each of the recordings in 0.2 mM Ca^{2+}. ***B***, The quantal content of the EPSCs is plotted against $[Ca^{2+}]_e$ (gray) and Q_{Ca} (the Ca current integral; black). All three are normalized to the 0.2 mM Ca^{2+} condition. The relationships are fit well by a Hill function with a coefficient of ~5. ***C***, The release rate reflected by the EPSCs is plotted against $[Ca^{2+}]_e$ (gray) and Q_{Ca} (the Ca current integral; black). Again, release rate, $[Ca^{2+}]$, and Q_{Ca} are normalized to the 0.2 mM Ca^{2+} condition, and the relationships are well fit by a Hill function with a coefficient of ~5.

Results

The exocytotic machinery uses a conventional Ca^{2+} sensor that is saturated by physiological $[Ca^{2+}]_e$

At conventional synapses, a steep relationship between $[Ca^{2+}]_e$ and exocytosis is well described and is presumed to reflect the requirement for the binding of multiple Ca^{2+} to the vesicular sensor to initiate release (Dodge and Rahamimoff, 1967). We wished to determine whether the vesicular Ca^{2+} sensor at the RB synapse exhibited a similarly steep dependence on $[Ca^{2+}]_e$. To do this, we assayed AMPA receptor (AMPAR)-mediated EPSCs evoked by tail Ca currents as the $[Ca^{2+}]_e$ was varied between 0.2 and 2 mM (Fig. 1*A*) (we believe this to be the first time this classic experiment has been performed using a retinal synapse). To prevent rundown of synaptic transmission from affecting our measurements, only two $[Ca^{2+}]_e$ were used for each experiment: 0.2 mM and 0.4, 0.6, 1, or 2 mM. We analyzed only recordings in which at least 10 stable responses were observed in each solution. Transmission in 0.2 mM $[Ca^{2+}]_e$ exhibited a large and very consistent number of failures (42 ± 8%, $n = 20$ paired recordings), and EPSC and Ca current parameters for each recording were normalized to those measured in 0.2 mM $[Ca^{2+}]_e$.

The maximal tail current-evoked EPSC reflects the release of only ~60% of the readily releasable pool (RRP) of vesicles ($n = 9$, data not shown) (also see Singer and Diamond, 2006), and using a brief stimulus that does not deplete the RRP removes consideration of vesicle cycling from the interpretation of our experiments. Additionally, Ca tail currents are not contaminated by the H^+-dependent inhibition of the presynaptic Ca channels that arises at some retinal ribbon synapses after MVR of acidic glutamatergic vesicles (supplemental Fig. 1*A*,*B*, available at www.jneurosci.org as supplemental material) (DeVries, 2001; Palmer et al., 2003). Further, we find that the recorded presynaptic currents reflect accurately the underlying Ca conductance changes mediating exocytosis; i.e., our voltage-clamp is adequate (supplemental Fig. 1*C*,*D*, available at www.jneurosci.org as supplemental material).

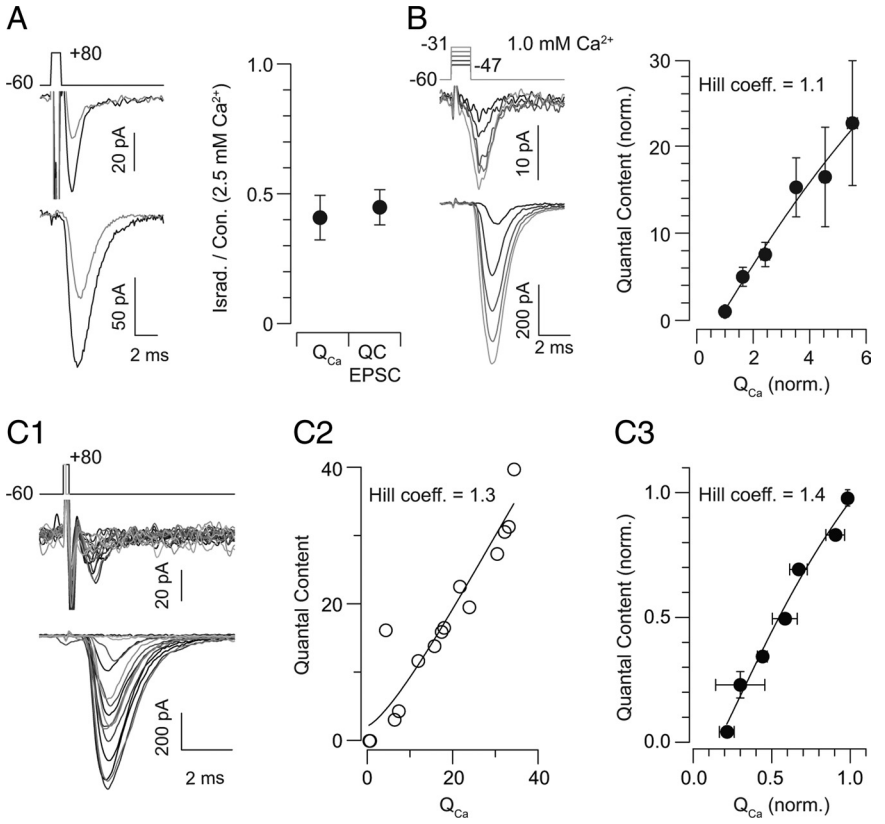

Figure 2. Exocytosis varies linearly with the number of open Ca channels. ***A***, In a saturating $[Ca^{2+}]_e$, application of the Ca channel antagonist isradipine reduces presynaptic Ca influx and EPSC quantal content equivalently (to 41 ± 7% and 45 ± 9% of control, and Q_{Ca} and EPSC quantal content, respectively; $n = 3$). Representative traces are on the left (black = control; gray = isradipine, 3 μM), and summary data are on the right. ***B***, Presynaptic voltage steps (1.5 ms) from −60 mV to potentials between −47 and −31 mV [in 4 mV increments; grayscale from −47 mV (dark) to −31 mV (light)] elicit Ca currents (top) and EPSCs (bottom). At right, EPSC quantal content is plotted against Q_{Ca}, illustrating a near-linear relationship between Ca^{2+} influx and exocytosis when the number of open presynaptic Ca channels is altered. Data are normalized to the condition of the smallest voltage step, in which 44 ± 5% of responses are failures of transmission ($n = 10$). $[Ca^{2+}]_e = 1$ mM. ***C1***, Presynaptic voltage steps of increasing duration (0.1–0.3 ms) from −60 to +80 mV elicit Ca tail currents and EPSCs of increasing amplitude ($[Ca^{2+}]_e = 1$ mM). ***C2***, The relationship between EPSC quantal content and presynaptic Ca charge transfer observed in a single cell is approximately linear and described by a Hill function with a coefficient of 1.3. ***C3***, A summary of the quantal content–Q_{Ca} relationship: data from each recorded pair were normalized to the maximal response recorded in that pair; data then were binned in increments of 0.15. The binned data are fit well by a Hill function with a coefficient of 1.3 ($n = 3$ recorded pairs).

We plotted both the quantal content of and the peak release rate [estimated by de-convolving the average quantal miniature EPSC (mEPSC) from the EPSC] (Singer et al., 2004) reflected by EPSCs against the normalized Ca current integral (Q_{Ca}) (Fig. 1*B*,*C*) and found that the relationship between Ca^{2+} influx and exocytosis was well described by a Hill function with a coefficient ≈5. Our observation is consistent with previous studies of other ribbon synapses: exocytosis evoked by photolysis of "caged" Ca^{2+} appears to require the binding of multiple (4–5) Ca^{2+} to a vesicular sensor (Heidelberger et al., 1994; Beutner et al., 2001). RBs express synaptotagmin 1 (Fox and Sanes, 2007), and we presume that this molecule acts as a Ca^{2+} sensor for exocytosis at this ribbon synapse as it does at many conventional synapses.

Additionally, we found that the exocytotic process appeared near saturation at 1 mM $[Ca^{2+}]_e$, close to the physiological $[Ca^{2+}]_e$ in the retina (Ames and Nesbett, 1981). Supporting this notion, the paired-pulse ratio (PPR) of the amplitudes of two EPSCs evoked 100 ms apart tracked the EPSC–$[Ca^{2+}]_e$ relationship closely and did not decline at $[Ca^{2+}]_e > 1$ mM, indicating that release probability did not increase at elevated $[Ca^{2+}]_e$ (PPR = 0.39 ± 0.1 at 1 mM and 0.45 ± 0.1 at 2 mM Ca^{2+}; $p = 0.46$; $n = 9$ paired recordings). Though it is thought that postsynaptic AMPARs at the RB–AII synapse are not saturated by MVR (Singer et al., 2004; Singer and Diamond, 2006; Singer, 2007), we thought it necessary to confirm that postsynaptic receptor saturation did not distort our measurements of the EPSCs at higher $[Ca^{2+}]_e$. We did this in two ways, and the resulting data are presented in supplemental Figure 2 (available at www.jneurosci.org as supplemental material). These observations confirm that the plateau of the relationship between the EPSC and $[Ca^{2+}]_e$ reflects saturation of the release machinery at physiological $[Ca^{2+}]_e$. In this respect, the RB synapse differs significantly from hair cell ribbon synapses as well as conventional synapses (Schneggenburger et al., 1999; Brandt et al., 2005).

A linear relationship between the number of open channels and the EPSC

As exocytosis from the presynaptic RB AZ appears to be steeply dependent on Ca^{2+} flux through presynaptic Ca channels, next we explored the possibility that $[Ca^{2+}]$ nanodomains generated by the opening of single channels control individual release sites. To do this, we altered presynaptic Ca^{2+} influx by changing the number of open Ca channels and examined concomitant changes in the EPSC (Brandt et al., 2005; Gentile and Stanley, 2005; Shahrezaei et al., 2006; Bucurenciu et al., 2010). Three experiments were performed. In experiment 1, in a saturating (2.5 mM) $[Ca^{2+}]_e$, we applied a low concentration (3 μM) of the Ca channel antagonist isradipine, sufficient to block the Ca current by ~50%. As isradipine antagonizes Ca channels by inducing entry into an inactivated (i.e., nonconducting) state, this manipulation effectively prevents some portion of the channels from contributing any Ca^{2+} to the release process (Berjukow et al., 2000; Hering et al., 2005). Thus, if Ca^{2+} flux through individual channels controls exocytosis from individual release sites, this manipulation should reduce the EPSC by ~50% despite the fact that the remaining Ca current is equivalent in amplitude to the Ca current recorded in 1.25 mM $[Ca^{2+}]_e$, a near-saturating $[Ca^{2+}]_e$. Indeed, isradipine blocked the EPSC by 45 ± 9% as it reduced the Ca current by 41 ± 7%, suggesting a 1:1 relationship between the number of open Ca channels and the number of release sites activated ($n = 3$) (Fig. 2*A*).

In experiment 2, we changed the number of open channels by delivering brief (1–2 ms) presynaptic voltage steps of varying amplitude. These step activated varying numbers of channels, and exocytosis was evoked primarily during the Ca current tail, when the driving force on Ca^{2+} was constant (Fig. 2*B*). The amplitude of evoked EPSCs varied with the magnitude of the presynaptic depolarization. From recording to recording, we observed a consistent number of failures of transmission after the smallest voltage step (44 ± 5% of responses; $n = 10$ recorded

pairs). Therefore, we normalized the Ca current and EPSC measurements for each recording to the values of the responses to the smallest step. The relationship between EPSC quantal content and Q_{Ca} (integrated over the entire step, not just the current tail) is plotted in Figure 2*B*: it is nearly linear and described by a Hill function with a coefficient of 1.1.

In experiment 3, we changed the number of open channels by eliciting Ca tail currents with voltage steps of varying length (0.1–0.3 ms) (Fig. 2*C*) (Llinás et al., 1981; Gentile and Stanley, 2005). Lengthening the duration of depolarization increased the number of presynaptic Ca channels activated and therefore raised the amplitude of the EPSC (Fig. 2*C*1). In performing these experiments, we were able to elicit Ca currents and EPSCs of a range of amplitudes within a single recorded pair. Consequently, we could plot the relationship between EPSC quantal content and presynaptic Q_{Ca} for each recorded pair (e.g., Fig. 2*C*2). These relationships were described by Hill functions with coefficients near 1 (for $n = 3$ recorded pairs, the Hill coefficients were 1.3, 1.6, and 1.4). In performing these experiments, we found it difficult to adjust the duration of the briefest voltage steps to yield a consistent number of failures of transmission (as described above). Therefore, to summarize the results of these experiments, we normalized the Ca current and EPSC measurements to the responses elicited by the longest voltage step and binned the data in increments of 0.15 to average between recorded pairs (Fig. 2*C*3). The relationship between average EPSC quantal content and average Q_{Ca} was approximately linear and described by a Hill function with a coefficient of 1.4 ($n = 3$).

It seems, then, that the opening of single Ca channels controls the release of individual vesicles (Yoshikami et al., 1989; Quastel et al., 1992; Bertram et al., 1999). The spatial relationship between Ca channels and release sites was investigated further with an additional series of experiments supplemented by simple simulations (supplemental Fig. 3, available at www.jneurosci.org as supplemental material). This supplementary line of inquiry provides additional support for our conclusion that the dynamics of transmission at the RB–AII synapse derive from the close coupling between Ca channels and release sites. Next, though, we wished first to determine the number of Ca channels open at the presynaptic terminal and second to determine whether we could observe directly exocytosis evoked by the opening of a single Ca channel using a physiologically relevant presynaptic stimulus.

Ca channel conductance

To determine the number of presynaptic Ca channels activated by our voltage stimuli, we estimated the charge flux through a single Ca channel by nonstationary variance (NSV) analysis of macroscopic Ca currents recorded in the whole-cell configuration from RB terminals (Sigworth, 1980). This task was facilitated by the use of transgenic mice in which ON bipolar cells, including RBs, express GFP, making it possible to visualize RB terminals and target them for recording (Morgan et al., 2006).

A train of five to six voltage steps (2–10 ms with a 55 ms interpulse interval, repeated at least 20 times) from −60 to −30 mV was used to depolarize RBs and elicit Ca currents. $[Ca^{2+}]_e$ was 2.5 mM to increase Ca current amplitude. We calculated the current variance as the averaged square of the difference between each individual response (not leak subtracted) (Roberts et al., 1990). The averaged leak-subtracted (P/4; 4 trains of 5–6 steps to −67.5 mV were applied; the step duration and interpulse interval were 2–10 and 55 ms, respectively) current–variance relationship was binned (20 bins) and plotted (Fig. 3*B*). The relationship was observed to be nonparabolic, indicating a low maximal open probability ($P_{open,max}$) for the Ca channels. Therefore, the single-channel current was taken as the slope of a line fit to the data. Fitting was performed only on data points acquired >1 ms after the voltage step to avoid contamination by any variance associated with transient capacitative currents. It is important to note that changes in variance were not associated with the purely passive currents evoked for leak subtraction, which decayed rapidly and with a monoexponential time course ($\tau < 0.2$ ms) (Fig. 3*C*).

Further, in these experiments, data were filtered at 8 kHz and acquired at 50 kHz. Because the average Ca channel open time is fairly short (~1 ms) (Fox et al., 1987), we took care to set the filter at more than five times the inverse of the channel open time to avoid attenuating the estimated current amplitude arising from brief channel openings (Silberberg and Magleby, 1993). We note that current–variance relationships were unaffected by changing the frequency at which the recordings were filtered (between 4 and 8 kHz; data not shown). Additionally, by recording from the axon terminals directly, we reduced the possibility that electrotonic filtering of single-channel currents would attenuate their estimated amplitudes.

The average single-channel current was -0.4 ± 0.1 pA ($n = 6$; mean ± SD). Taking E_{Ca} as +90 mV, approximately equivalent to the thermodynamic E_{Ca}, the single-channel conductance is ~3 pS. This measurement is consistent with that reported for a study of presynaptic L-type single-channel currents in the chick ciliary ganglion (Church and Stanley, 1996). Thus, to estimate the single-channel current at multiple $[Ca^{2+}]_e$, we made use of the formulation presented by Church and Stanley (1996): conductance in pS $= 9.2/(1 + 5.6/[Ca^{2+}]_e)$. Given that the average tail Ca current amplitude in 2.5 $[Ca^{2+}]_e$ is -52 ± 7 pA ($n = 14$ somatic recordings) and a single RB terminal contains ~40 separate AZs (Tsukamoto et al., 2001; Singer et al., 2004), we calculate that only approximately three to four channels open per AZ at the peak of a tail Ca current. More physiological stimuli, which may not reach levels of depolarization sufficient to achieve maximal channel open probability, then are likely to activate fewer than three channels/AZ.

To confirm the validity of our measurements, we performed two control experiments. In one, we repeated our measurements of single-channel current amplitude in the presence of the dihydropyridine agonist BayK8644 (BayK; 10 μM) (Fig. 3*D*,*E*). BayK increases channel open probability and mean open time without affecting single-channel conductance (Brown et al., 1984; Hess et al., 1984) (but, see Tavalin et al., 2004). Accordingly, Ca currents recorded in the presence of BayK were larger than those recorded in control conditions though the current–variance relationship remained nonparabolic ($p = 0.03$ by ANOVA; 70 ± 5 vs 53 ± 3 pA, BayK vs control; $n = 9$ and 6, respectively), but the average single-channel current measured in the presence of BayK was statistically indistinguishable from that measured in control conditions (0.4 ± 0.1 pA; mean ± SD; $p = 0.23$ by ANOVA).

In the second control experiment, we repeated our measurements in the presence of a non-dihydropyridine agonist of L-type currents, FPL 64176 (FPL; 5 μM) (Fig. 3*F*,*G*). FPL both increases the single-channel conductance and slows channel activation and deactivation (Handrock et al., 1998; Fan et al., 2001) (but, see Liu et al., 2003; Tavalin et al., 2004), and we expected that this manipulation would increase the measured single-channel current. Ca currents recorded in the presence of FPL, and 2.5 mM Ca^{2+} currents were larger and slower than control currents. The current–variance relationship remained nonparabolic in FPL, and the single-channel current estimated from a line fit to the data points was -0.7 ± 0.2 pA (mean ± SD; $n = 7$) (Fig. 3*E*).

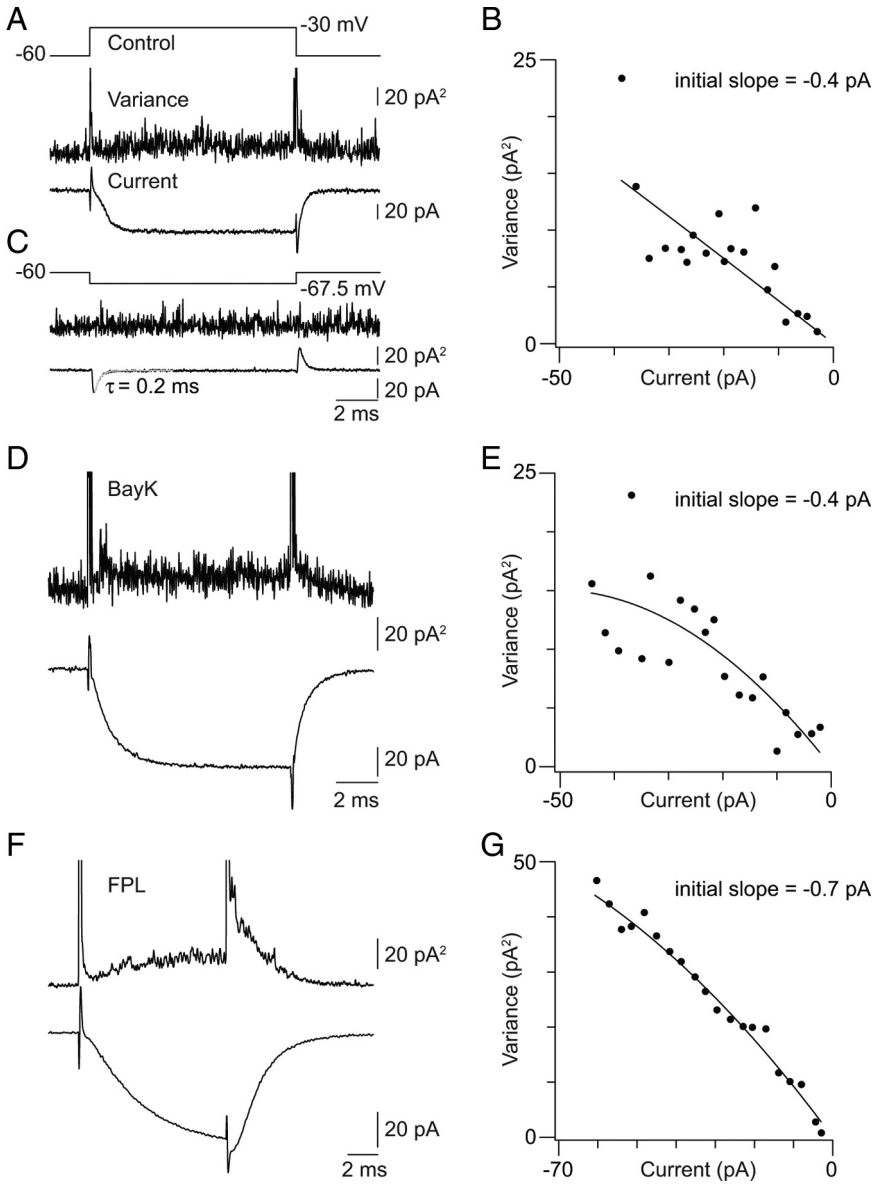

Figure 3. Estimation of the single Ca channel current; $[Ca^{2+}]_e = 2.5$ mM. ***A***, Average trial-to-trial variance (middle trace) and current (leak subtracted, bottom trace) elicited by a 10 ms step from −60 to −30 mV (top trace). ***B***, The binned current–variance relationship for the recording illustrated in ***A***. ***C***, Changes in current variance are not associated with voltage steps that do not activate Ca currents. The voltage step used for P/4 leak subtraction of the current illustrated in ***A*** is shown. ***D***, Ca current (leak subtracted) and variance around the mean elicited by a 10 ms voltage step in the presence of 10 μM BayK. ***E***, The binned current–variance relationship for the recording illustrated in ***D***. Note that BayK does not increase the measured single Ca channel current. ***F***, Ca current (leak subtracted) and variance around the mean elicited by a 10 ms voltage step in the presence of 5 μM FPL. Note the slowed activation and deactivation of the current. ***G***, The current–variance relationship for the recording illustrated in ***F***. Note the increased single Ca channel current observed in the presence of FPL.

The reported effects of BayK and FPL on single-channel conductance vary with the charge carrier (Ca^{2+} or Ba^{2+}) and with experimental system, leading to the reasonable suggestion that these agents exert differential effects on different Ca channel α subunits (Tavalin et al., 2004). The subunit composition of the presynaptic Ca channel in the RB terminal is not certain; antibody-labeling studies have identified both Cav1.2 and Cav1.4 as candidates for the α subunit (Berntson et al., 2003; Rieke et al., 2008). Single Ca channel conductance in cardiomyocytes, which express Cav1.2, is unaffected or minimally affected by BayK and enhanced substantially by FPL (Hess et al., 1984; Lacerda and Brown, 1989; Handrock et al., 1998; Fan et al., 2001); BayK has a very small effect on single-channel conductance of recombinant Cav1.4-containing channels (Doering et al., 2005); the effects of FPL on Cav1.4-containing channels are unexplored. Comparison of the results presented here (Fig. 3) with future studies of agonist effects on recombinant receptors, then, may provide some insight into the molecular composition of the Ca channels in RB terminals.

Desynchronizing exocytosis allows the presynaptic voltage threshold for exocytosis to be determined reliably

To determine the minimum number of presynaptic Ca channels that must be activated to elicit exocytosis, we applied a slow voltage ramp (−60 to −45 mV at 0.6 mV/ms) to the soma of the presynaptic RB and recorded EPSCs in the postsynaptic AII. Evoked release was desynchronized, as has been described previously (Singer et al., 2004; Snellman et al., 2009), and we were able to examine the timing and amplitude of individual EPSCs (Fig. 4). We formulated two hypotheses: (1) that if the opening of a single channel could evoke exocytosis, we would observe EPSCs first at a threshold presynaptic voltage at which <1 Ca channel/AZ on average was open; and (2) that if the opening of a single channel could evoke exocytosis, the probability of observing EPSCs at this threshold would increase with $[Ca^{2+}]_e$ though the threshold itself would remain constant (i.e., the number of open channels remains constant with varying $[Ca^{2+}]_e$, but the probability that a channel opening will evoke an EPSC increases with Ca^{2+} flux through individual channels).

To address these hypotheses experimentally, we examined EPSCs evoked by ramps performed when $[Ca^{2+}]_e$ was increased from 0.4 to 0.8 mM (Fig. 4*A*); this concentration range encompasses the very steep portion of the $[Ca^{2+}]_e$/EPSC relationship (Fig. 1). We measured the amplitudes of the individual EPSCs evoked by each trial as well as the presynaptic voltage at which each EPSC occurred. EPSC amplitudes were normalized to the average mEPSC amplitude recorded in each cell and plots of amplitude versus presynaptic voltage are illustrated in Figure 4*B*. EPSCs became evident first at approximately −56 mV, at which point the presynaptic Ca current had an amplitude of ~1 pA, corresponding to the opening of three to four channels distributed among the 40 RB AZs (i.e., there are ~0.1 open channels/AZ, assuming a single-channel current of 0.12 pA at 0.8 mM $[Ca^{2+}]$ and 0.06 pA at 0.4 mM $[Ca^{2+}]$). Assuming that channel opening is a stochastic process described by Poisson statistics, the probability of two Ca channels being open simultaneously at the same presynaptic AZ when 0.1 chan-

nels/AZ open on average is <0.005. Because a single RB contacts a single AII ~10 times (Tsukamoto et al., 2001; Singer et al., 2004), it is likely that at this membrane potential, there is a single open Ca channel at only one of the AZs presynaptic to the recorded AII.

For each trial, we determined the presynaptic voltage at which the first EPSC was observed, and we plotted histograms of EPSCs versus presynaptic voltage in 2 mV bins (Fig. 4*C*). It is apparent that at both $[Ca^{2+}]_e$ values a significant fraction of EPSCs is evoked first when the presynaptic voltage is between −57 and −50 mV, and the percentage of first events observed in this range increases with Ca^{2+} flux through individual channels as $[Ca^{2+}]_e$ is raised. Specifically, EPSCs were observed in 25/170 trials (15%) conducted in 0.4 mM $[Ca^{2+}]_e$ and in 77/170 trials (45%) when $[Ca^{2+}]_e$ was raised to 0.8 mM. Because in these experiments the RB voltage is maintained between −60 and −50 mV for ~17 ms (the ramp rate is 0.6 mV/ms), far longer than the mean open time of a neuronal L-type Ca channel (Nowycky et al., 1985; Fox et al., 1987), it is impossible to determine the probability with which the opening of a single Ca channel evokes exocytosis. Our observations, however, suggest that Ca^{2+} influx through a single Ca channel can evoke exocytosis reliably.

Additionally, it is notable that the EPSCs evoked at threshold have amplitudes similar to those of mEPSCs and therefore are likely uniquantal. Multiquantal events are observed only after the presynaptic voltage has become more depolarized and the presynaptic Ca current has become larger (corresponding to the opening of ~1 channel/AZ). The average EPSC amplitude (binned over 3 mV increments) and the average Ca current are plotted against presynaptic voltage in Figure 4*D*. We were intrigued by the observation that multiquantal events were not evident when a single-channel opening triggered exocytosis and wished to determine whether single-channel openings would evoke MVR by elevating $[Ca^{2+}]$ concomitantly at multiple release sites were Ca^{2+} flux through the channels increased or intraterminal Ca^{2+} buffer capacity decreased. Therefore, we repeated the ramp experiment described above under two experimental conditions: (1) in the presence of a saturating $[Ca^{2+}]_e$ of 2.5 mM; and (2) with 0.1 mM BAPTA in the pipette solution to reduce the Ca^{2+} buffering capacity of the presynaptic terminal.

With 2.5 mM $[Ca^{2+}]_e$, release events evoked at presynaptic potentials <−50 mV (corresponding to the opening of ~0.1 channels/AZ) were observed in all trials (160 events in 134 trials). Again, because there may be multiple Ca channel openings throughout the duration of the presynaptic stimulus, we cannot determine the number of openings that precede each release event. The median presynaptic voltage at which the first EPSC was evoked, however, was more hyperpolarized than in 0.4 or 0.8 mM (Fig. 4*B*,*C*), consistent with the notion that increasing Ca^{2+} influx through individual channels increases the probability that a vesicle at a nearby release site will undergo exocytosis. The amplitudes of EPSCs evoked at potentials hyperpolarized to −50 mV, however, remained equivalent to those of quantal mEPSCs (Fig. 4*B*,*D*). Similarly, reducing the exogenous buffer concentration in the presynaptic terminal 10-fold, to 0.1 mM BAPTA ($[Ca^{2+}]_e$ = 1 mM), did not affect amplitudes of release events evoked by depolarization to potentials <−50 mV (Fig. 4*B*,*D*) (events were seen in 18/47, or 38%, of trials). These observations support the notion that the opening of a single Ca channel at a

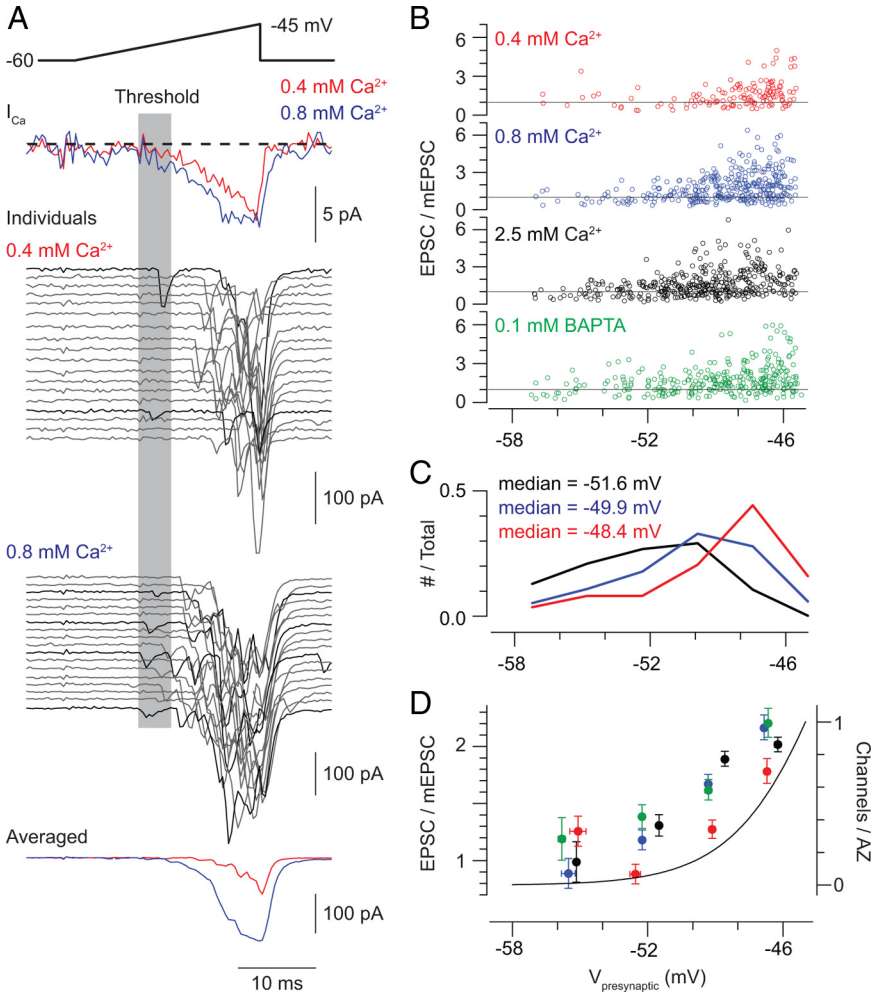

Figure 4. Voltage-ramp stimuli reveal the presynaptic voltage threshold for exocytosis. ***A***, Ramp depolarization from −60 to −45 mV elicits presynaptic Ca currents (top) and evoked EPSCs (below). Individual (middle) and averaged (bottom) responses recorded in 0.4 and 0.8 mM Ca^{2+} are illustrated. It is possible to identify trials in which evoked transmission occurs at the voltage threshold for Ca current activation (black). ***B***, For three $[Ca^{2+}]_e$ (0.4, 0.8, and 2.5 mM) with 1 mM BAPTA in the pipette solution and for one $[Ca^{2+}]_e$ (1 mM) with 0.1 mM BAPTA in the pipette solution, the amplitudes of each evoked EPSC are normalized to the average mEPSC amplitude (for each cell) and plotted against the presynaptic voltage (data pooled from 3 recorded pairs for each condition). It is obvious that multiquantal EPSCs are evoked only at potentials depolarized to the threshold for exocytosis. ***C***, The voltages at which the first evoked response is observed during recordings in 0.4, 0.8, and 2.5 mM Ca^{2+} are displayed; voltages are binned in increments of 2 mV (n = 3 paired recordings for each condition). In all conditions, release events are observed at the threshold for Ca current activation, but the frequency of observing events at this threshold increases with $[Ca^{2+}]_e$. ***D***, Averaged EPSC amplitudes for each experimental condition (normalized to mEPSC amplitude; left-hand y-axis) and the estimated number of open Ca channels per AZ (calculated by dividing the average of ramp-evoked Ca currents recorded in 9 RBs in 2.5 mM Ca^{2+} by the single-channel current measured by NSV and then by 40—the estimated number of presynaptic AZs; green trace, right-hand y-axis) plotted against presynaptic membrane potential. Data are binned in 3 mV increments.

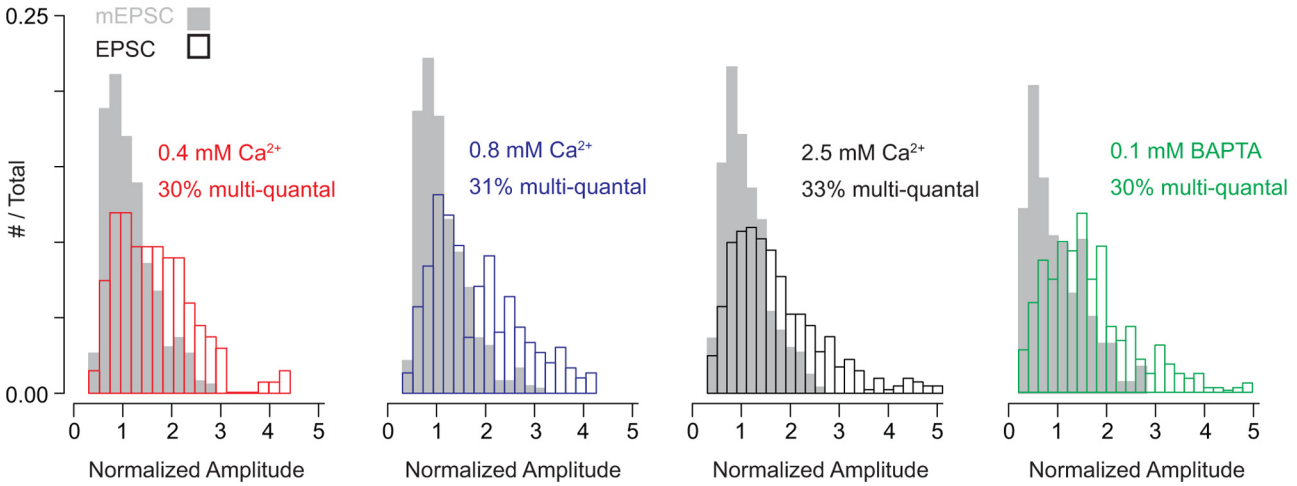

Figure 5. Approximately 30% of evoked events are multiquantal. Histograms of mEPSC (gray bars) and ramp-evoked EPSC (open bars) amplitudes (normalized to mean mEPSC amplitude) recorded in 0.4, 0.8, and 2.5 mM Ca^{2+} and in 1 mM Ca^{2+} with 0.1 mM BAPTA in the presynaptic pipette. Distributions reflect data pooled from 3 recorded pairs in each condition. For all conditions, ~30% of the evoked events are multiquantal, as determined by calculating the area of the evoked event distribution that does not overlap with the mEPSC distribution.

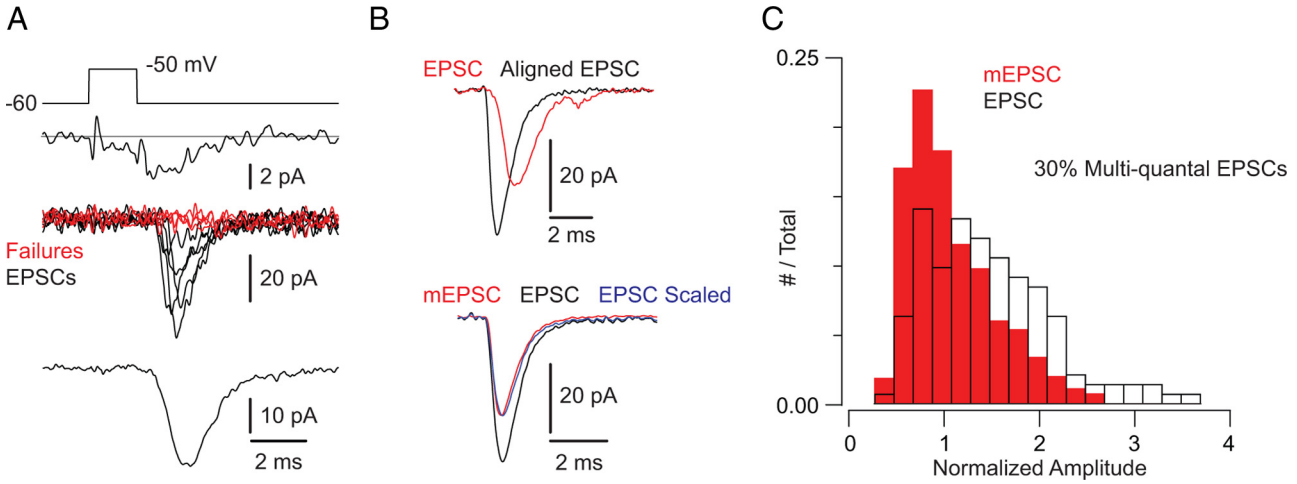

Figure 6. Multiquantal EPSCs evoked by the opening of ~1 channel/AZ. ***A***, A 10 mV, 1.5 ms presynpatic depolarization elicits small presynaptic tail Ca currents (top) and evokes EPSCs with a high percentage of failures of transmission (middle: individual EPSCs; bottom: average of all events including failures). ***B***, There is substantial jitter in evoked transmission. Top, If evoked events are aligned at their starting points, the averaged EPSC waveform is larger and faster (black) than the nonaligned average (red). Bottom, The aligned and averaged EPSC (black) is larger than the quantal mEPSC (red) but has the identical time course, as illustrated by the scaled trace (blue). ***C***, Evoked EPSC and mEPSC distributions (data pooled from 4 recorded pairs; EPSCs and mEPSCs normalized to the mean mEPSC amplitude) illustrate that 30% of the evoked events are multiquantal, as determined by calculating the area of the evoked event distribution that does not overlap with the mEPSC distribution.

single AZ is sufficient to elicit exocytosis of a single vesicle but is insufficient to elevate $[Ca^{2+}]$ at multiple release sites and thereby support MVR.

MVR appears to require the opening of multiple channels/AZ

We observed in all $[Ca^{2+}]_e$ that multiquantal events occurred only when the presynaptic voltage was depolarized to −50 mV (Fig. 4*B*,*D*). At this potential, one Ca channel on average opens at each AZ. When an ensemble current arises from the contribution of, on average, one stochastic channel opening/AZ, Poisson statistics predict that 26% of AZs will contribute more than one open channel (and 35% of AZs will have no open channels). As exocytosis at the RB synapse is a binomial process (Singer et al., 2004), we postulated that slightly more than one-quarter of the evoked EPSCs that we recorded would be multiquantal if the opening of multiple Ca channels was required to evoke MVR.

Indeed, we found this to be the case. To estimate the number of multiquantal events, we calculated the area of the evoked EPSC distribution that did not overlap with the mEPSC distribution (both distributions contained normalized data pooled from multiple recordings and were significantly different as determined by the Mann–Whitney *U* test). The percentage of multiquantal events was similar in different $[Ca^{2+}]_e$ and was close to the percentage of AZs predicted to have at least two open Ca channels: 30% in 0.4 mM, 31% in 0.8 mM, 33% in 2.5 mM $[Ca^{2+}]_e$, and 30% in 1 mM $[Ca^{2+}]_e$ with 0.1 mM internal BAPTA (Fig. 5).

To provide additional evidence for the assertion that the extent of evoked MVR is determined by the opening of multiple Ca channels at an AZ, we evoked EPSCs using a different experimental protocol. The presynaptic RB was depolarized in 1 mM Ca^{2+} to −50 mV for 1.5–2 ms to activate few Ca channels; EPSCs were evoked during the tail Ca current that was elicited (Fig. 6). This protocol generated small Ca currents (3.6 ± 0.2 pA, reflecting the opening of ~0.6 channels/AZ; $n = 4$), and failures of transmission were seen in ~50% of trials. Evoked events were largely monophasic (i.e., they exhibited a rising phase with no obvious

inflections and a smooth, monoexponential decay), but significant jitter in the timing of individual synaptic events was observed. The extent of this jitter is obvious when individual EPSCs are averaged after being aligned at their starting points: the resultant trace is larger and faster to rise and decay than an averaged trace generated without alignment of individual events (Fig. 6*Bi*).

Despite the jitter in the timing of the exocytotic events, individual EPSCs rose rapidly and had waveforms indistinguishable from quantal mEPSCs despite their being larger on average (quantal content = 1.2 ± 0.1 quanta; $n = 4$ recorded pairs). This is evident in a comparison of the aligned and averaged EPSC and mEPSC waveforms (aligned EPSC vs mEPSC: 10–90% rise time = 0.4 ± 0.1 vs 0.3 ± 0.1 ms, $p = 0.22$ by Mann–Whitney U test; τ_{decay} = 1.0 ± 0.2 vs 0.8 ± 0.1 ms, $p = 0.23$; $n = 4$ recorded pairs) (Fig. 6*B*). This suggests the action of coordinated MVR, as has been described previously (Singer et al., 2004).

Further, for each recording EPSC amplitudes were normalized to the average mEPSC amplitude, and data from multiple recordings were pooled to generate normalized mEPSC and EPSC amplitude histograms (Fig. 6*C*). When we assayed the area of the EPSC amplitude histogram that did not include the mEPSC histogram, we found it to be 30%. This is close to the value of 26% predicted by the Poisson distribution of open Ca channels at AZs when the average number of open channels is ~1/AZ.

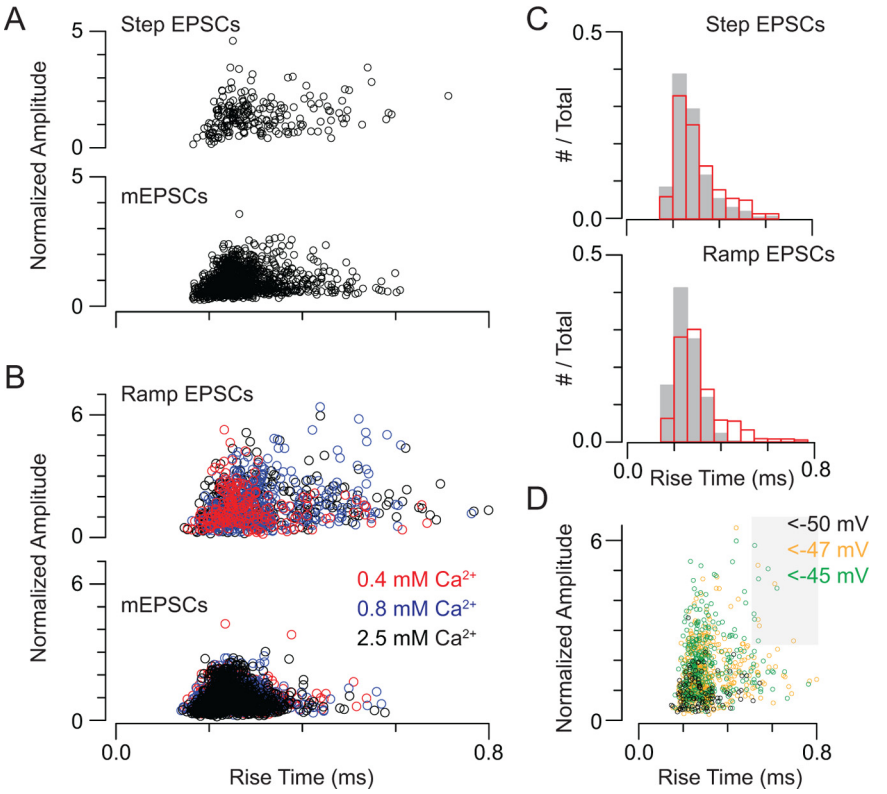

Figure 7. Multiquantal EPSCs have fast rise times. ***A***, Amplitude–rise time relationship for step-evoked EPSCs and mEPSCs recorded in the same experiment. Data are pooled from 4 recorded pairs, and amplitudes are normalized to the mean mEPSC amplitude. ***B***, Amplitude–rise time relationship for ramp-evoked EPSCs and mEPSCs recorded in the same experiment. Recordings in various $[Ca^{2+}]_e$ are differentiated by color. Data are pooled from 6 recorded pairs, and amplitudes are normalized to the mean mEPSC amplitude. ***C***, Histograms of EPSC and mEPSC rise times for experiments in which EPSCs were evoked by small presynaptic voltage steps (top) and presynaptic voltage ramps (bottom). ***D***, Plot of EPSC amplitude versus rise time; color code reflects the presynaptic voltage at which the EPSC was evoked. It is evident that large EPSCs are not recorded at presynaptic potentials < -50 mV, and that large, slow EPSCs can be evoked at all potentials > -50 mV. The gray area denotes EPSCs with amplitude >2.5 quanta and rise time >0.5 ms (2 SDs above the mean).

Because ~70% of the evoked events that we recorded appeared to reflect the release of single vesicles, the waveform of the averaged EPSC is dominated by the time courses of quantal events. Therefore, we wished to confirm that multiquantal EPSCs do not have a markedly different time course from uniquantal EPSCs. We did this by examining the waveforms of individual evoked and spontaneous (quantal) EPSCs (Fig. 7). We plotted the relationship between rise time (10–90%) and amplitude for EPSCs evoked by either small presynaptic voltage steps (e.g., Fig. 6) or presynaptic ramps (e.g., Fig. 4) as well as for the mEPSCs recorded in the corresponding experiments.

By comparing amplitude–rise time relationships of EPSCs and mEPSCs (Fig. 7*A*,*B*) and rise-time histograms of EPSCs and mEPSCs (Fig. 7*C*), it is apparent that the majority of EPSCs (both step evoked and ramp evoked) have rise times equivalent to those of mEPSCs. A subset of evoked events rose slightly more slowly than did mEPSCs, making the EPSC and mEPSC rise-time distributions statistically different ($p \ll 0.05$ by Mann–Whitney U test). The largest EPSCs, however, were not uniformly slower than uniquantal events.

To support this conclusion, we examined ramp-evoked EPSCs in some detail. Of the 886 recorded EPSCs, 241 (27%) had quantal contents >2.5. The average rise time of these events was 0.3 ± 0.1 ms (mean ± SD; compared with 0.3 ± 0.1 ms for the events with quantal content <2.5; the average mEPSC rise-time = 0.3 ± 0.1 ms). Only 12/241 large, multiquantal EPSCs had rise-times >0.5 ms (>2 SDs above mean) (Fig. 7*D*, shaded area). This represents only 5% of the large EPSCs (and 1% of the total). These large, slower EPSCs were evoked at all membrane potentials > -50 mV (the threshold for MVR) and < -45 mV (the most depolarized potential reached by the ramp); they did not occur only at the end of the presynaptic voltage ramp (-45 mV) where the release rate was the highest, and EPSCs often were superimposed upon each other (Fig. 7*D*). Thus, from this analysis we conclude that the multiquantal EPSCs that we recorded reflect multivesicular release that is coordinated on a time scale <100–150 μs (2–3 sampling intervals at our sampling rate of 20 kHz); this is consistent with a previously published study (Singer et al., 2004).

Discussion

Our study elucidates a synaptic mechanism—nanodomain control of exocytosis—that underlies the physiological behavior of the RB synapse. Nanodomain control broadens the operating range of the synapse by generating a near-linear relationship between presynaptic membrane potential and exocytosis. Further, it permits a transition from uniquantal to multiquantal release to occur when multiple Ca channels/AZ open; this likely serves to increase synaptic gain at visual threshold. Importantly, MVR is not elicited by the opening of a single Ca channel.

Inferring the distribution of Ca channels at the presynaptic AZ

Approximately five Ca channels are associated closely with each docked vesicle at the RB AZ (Raviola and Raviola, 1982; von Gersdorff et al., 1998). As the RRP size at each AZ is approximately eight to nine vesicles, 45–50 Ca channels may be located at each AZ (data not shown) (Singer and Diamond, 2006; Zhou et al., 2006). Because approximately three channels/AZ open at the peak of a Ca tail current (Fig. 3), $P_{open,max}$ for these channels must be quite low (~5–10%). This is consistent with a study of the frog neuromuscular junction, another synapse at which few or single Ca channels control the release of single vesicles (Shahrezaei et al., 2006). During a physiological depolarization, then, only one or two channels/AZ will open coincidently.

Colocalization of Ca channels and vesicles is consistent with a synapse at which release sites are controlled by the opening of one or few Ca channels (Stanley, 1993; Brandt et al., 2005; Fedchyshyn and Wang, 2005; Shahrezaei et al., 2006; Bucurenciu et al., 2010). A previous study provides evidence for such colocalization in RB terminals: exocytosis at this synapse is largely insensitive to the exogenous Ca^{2+} chelators BAPTA and EGTA (Singer and Diamond, 2003). Here, two novel pieces of evidence for close coupling between Ca channels emerge (Figs. 4, 5). One, exocytosis is evoked reliably at presynaptic voltages sufficient to open only a single Ca channel at a subset of AZs. Two, the percentage of evoked events that are multiquantal does not increase with Ca^{2+} influx, indicating that Ca^{2+} does not act at a distance from its site of entry. In this respect, Ca channel-release site coupling at the mammalian RB synapse differs from that of the well-studied goldfish retinal giant bipolar cell synapse, at which exocytosis of individual vesicles requires the opening of multiple (~5) channels (von Gersdorff and Matthews, 1997; von Gersdorff et al., 1998; Coggins and Zenisek, 2009).

We used simple simulations to assist in the interpretation of the data presented and to provide evidence that the combination of few open Ca channels located near a small RRP accounts for the dynamics of release from the RB terminal (supplemental Fig. 3, available at www.jneurosci.org as supplemental material). It is important to note that our observation that the opening of single Ca channels can activate individual release sites does not preclude the possibility that $[Ca^{2+}]$ domains arising from different channels may overlap (Stanley, 1993, 1997; Shahrezaei et al., 2006). Indeed, under conditions in which the RRP is full and approximately five presynaptic Ca channels are open (Figs. 1, 2) (e.g., when exocytosis is evoked by a tail Ca current), the mean distance between open channels is <20 nm, the average radius of a nanodomain generated by the opening of a single channel (supplemental Fig. 3, available at www.jneurosci.org as supplemental material). When only two channels/AZ open simultaneously, though (e.g., Figs. 4, 6), the mean distance between open channels is increased to 124 nm. Under this condition, which occurs at membrane potentials in the physiological operating range of the presynaptic terminal, <4% of open channels are within 20 nm of each other. Consequently, signaling during visual processing likely depends primarily on $[Ca^{2+}]$ nanodomain control of release sites.

Mechanisms of MVR

Coordinated MVR from auditory hair cells, rods, and RBs has been described (Glowatzki and Fuchs, 2002; Singer et al., 2004; Suryanarayanan and Slaughter, 2006; Li et al., 2009). The mechanism(s) underlying coordinated MVR are uncertain, and a universal one may not exist. For example, coordinated MVR from amphibian rods requires release of Ca^{2+} from internal stores (Suryanarayanan and Slaughter, 2006); store-mediated MVR has been observed in studies of cerebellar synapses but not in studies of auditory hair cell synapses (Llano et al., 2000; Neef et al., 2007).

Because the opening of single Ca channels does not evoke MVR even when Ca^{2+} flux through these channels saturates the vesicular release machinery (Figs. 1, 4), $[Ca^{2+}]$ must be elevated over an area larger than the domain of a channel to elicit MVR. Consistent with this notion, Ca^{2+}-dependent coordinated MVR occurs at RB synapses during asynchronous release after the closure of Ca channels, at which time channel micromains have dissipated but intraterminal $[Ca^{2+}]$ remains elevated (Singer et al., 2004). That the number of predicted multichannel openings is quite similar to the observed number of multiquantal evoked events (~30%) (Figs. 5, 6) indicates that the coordinating event requires the coincident elevation of $[Ca^{2+}]$ at multiple release sites. This mechanism, however, does not explain the precise timing of MVR (Fig. 6, 7): evoked multiquantal events have essentially the same time course as uniquantal mEPSCs though they exhibit significant intertrial jitter in their timing (Fig. 6, 7). Exocytotic events occurring at independent release sites, however, should exhibit jitter in their timing, and jitter is thought to arise downstream of Ca^{2+} binding to the release machinery (Diamond and Jahr, 1995; Isaacson and Walmsley, 1995).

Compound fusion, or the fusion of multiple vesicles to each other before a single exocytotic event, is a mechanism that can account for the precise timing of MVR. Direct evidence for compound fusion at a neuronal AZ, however, is rare. In a study of transmission at the Calyx of Held, He et al. (2009) observed an increase in quantal amplitude with no change in EPSC time course after long (up to 30 s) periods of presynaptic stimulation with either high-frequency action potential trains or KCl application. This phenomenon was interpreted to reflect compound fusion, a suggestion supported by the demonstration of a stimulation-induced increase in vesicle diameter. Similarly, increased vesicle size indicating compound fusion has been observed in the goldfish giant bipolar cell terminal after prolonged stimulation (Matthews and Sterling, 2008).

Though we have no direct experimental evidence supporting or discounting the contribution of compound fusion to coordinated MVR, three observations argue indirectly against compound fusion being the sole underlying mechanism. One, coordinated MVR follows the opening of only two Ca channels/AZ (Figs. 4, 6); our experimental paradigm is very different from the strong stimulation used in the aforementioned studies (Matthews and Sterling, 2008; He et al., 2009). It is improbable that neighboring channels always open together to promote fusion of adjacent vesicles, and the opening of two channels is unlikely to elevate $[Ca^{2+}]$ globally to promote compound fusion reliably. Two, though we would expect that compound fusion would increase with Ca influx into the RB terminal, neither the amplitude of multiquantal EPSCs (Fig. 5) nor the mEPSC amplitude (data not shown) (Singer et al., 2004) increases with $[Ca^{2+}]_e$. Three, it is unlikely that the appearance of multiquantal events in the EPSC distribution would be predicted by simple binomial statistics if vesicles fused with each other in addition to the plasma membrane (Singer et al., 2004). Thus, the precise mechanism of coordinated MVR at the RB synapse remains to be discovered. Though compound fusion cannot be discounted, other mechanisms also should be considered.

Relevance to scotopic signal processing

Signal gain in the neural circuitry downstream of rods appears to be controlled at the RB–AII synapse: at low light intensities—<1 rhodopsin isomerization (R*)/rod/s—the synapse amplifies RB responses and then reduces its gain as a result of synaptic depression (Dunn et al., 2006; Dunn and Rieke, 2008). The voltage dependence of the transition from uniquantal to multiquantal release that we describe here (Fig. 4) is well matched to serve the operational needs of the RB synapse. In the dark-adapted retina, the RB rests at −60 mV, the presynaptic holding potential in our experiments (Dunn and Rieke, 2008). EPSPs evoked in RBs at light intensities <1 R*/rod/s are not well characterized but are likely 5–10 mV (based on light-evoked EPSCs of 5–10 pA and an input resistance of ~1 GΩ) (Field and Rieke, 2002; Dunn and Rieke, 2008). Depolarization 5–10 mV from rest moves the RB membrane through the foot of the presynaptic Ca channel I–V relationship (a highly nonlinear range), making evoked exocytosis multiquantal as the probability of multiple Ca channel openings/AZ increases. The transition to MVR can provide significant amplification of the synaptic signal as the RB terminal traverses the voltage range likely to be covered by light responses elicited when rods absorb only single photons. At higher light intensities, RB output varies linearly with membrane potential: presynaptic voltage changes on the linear portion of the Ca channel I-V relationship, and exocytosis varies linearly with the number of activated Ca channels to provide a wide dynamic range for signaling.

References

Ames A 3rd, Nesbett FB (1981) In vitro retina as an experimental model of the central nervous system. J Neurochem 37:867–877.

Berjukow S, Marksteiner R, Gapp F, Sinnegger MJ, Hering S (2000) Molecular mechanism of calcium channel block by isradipine. Role of a drug-induced inactivated channel conformation. J Biol Chem 275: 22114–22120.

Berntson A, Taylor WR, Morgans CW (2003) Molecular identity, synaptic localization, and physiology of calcium channels in retinal bipolar cells. J Neurosci Res 71:146–151.

Bertram R, Smith GD, Sherman A (1999) Modeling study of the effects of overlapping Ca2+ microdomains on neurotransmitter release. Biophys J 76:735–750.

Beutner D, Voets T, Neher E, Moser T (2001) Calcium dependence of exocytosis and endocytosis at the cochlear inner hair cell afferent synapse. Neuron 29:681–690.

Bloomfield SA, Dacheux RF (2001) Rod vision: pathways and processing in the mammalian retina. Prog Retin Eye Res 20:351–384.

Brandt A, Khimich D, Moser T (2005) Few CaV1.3 channels regulate the exocytosis of a synaptic vesicle at the hair cell ribbon synapse. J Neurosci 25:11577–11585.

Brown AM, Kunze DL, Yatani A (1984) The agonist effect of dihydropyridines on Ca channels. Nature 311:570–572.

Bucurenciu I, Bischofberger J, Jonas P (2010) A small number of open Ca2+ channels trigger transmitter release at a central GABAergic synapse. Nat Neurosci 13:19–21.

Church PJ, Stanley EF (1996) Single L-type calcium channel conductance with physiological levels of calcium in chick ciliary ganglion neurons. J Physiol 496:59–68.

Coggins M, Zenisek D (2009) Evidence that exocytosis is driven by calcium entry through multiple calcium channels in goldfish retinal bipolar cells. J Neurophysiol 101:2601–2619.

DeVries SH (2001) Exocytosed protons feedback to suppress the Ca2+ current in mammalian cone photoreceptors. Neuron 32:1107–1117.

Diamond JS, Jahr CE (1995) Asynchronous release of synaptic vesicles determines the time course of the AMPA receptor-mediated EPSC. Neuron 15:1097–1107.

Dodge FA Jr, Rahamimoff R (1967) Co-operative action a calcium ions in transmitter release at the neuromuscular junction. J Physiol 193:419–432.

Doering CJ, Hamid J, Simms B, McRory JE, Zamponi GW (2005) Cav1.4 encodes a calcium channel with low open probability and unitary conductance. Biophys J 89:3042–3048.

Dulon D, Safieddine S, Jones SM, Petit C (2009) Otoferlin is critical for a highly sensitive and linear calcium-dependent exocytosis at vestibular hair cell ribbon synapses. J Neurosci 29:10474–10487.

Dunn FA, Rieke F (2008) Single-photon absorptions evoke synaptic depression in the retina to extend the operational range of rod vision. Neuron 57:894–904.

Dunn FA, Doan T, Sampath AP, Rieke F (2006) Controlling the gain of rod-mediated signals in the mammalian retina. J Neurosci 26:3959–3970.

Fan J, Yuan Y, Palade P (2001) FPL-64176 modifies pore properties of L-type Ca(2+) channels. Am J Physiol Cell Physiol 280:C565–572.

Fedchyshyn MJ, Wang LY (2005) Developmental transformation of the release modality at the calyx of Held synapse. J Neurosci 25:4131–4140.

Field GD, Rieke F (2002) Nonlinear signal transfer from mouse rods to bipolar cells and implications for visual sensitivity. Neuron 34:773–785.

Field GD, Sampath AP, Rieke F (2005) Retinal processing near absolute threshold: from behavior to mechanism. Annu Rev Physiol 67:491–514.

Fox AP, Nowycky MC, Tsien RW (1987) Single-channel recordings of three types of calcium channels in chick sensory neurones. J Physiol 394:173–200.

Fox MA, Sanes JR (2007) Synaptotagmin I and II are present in distinct subsets of central synapses. J Comp Neurol 503:280–296.

Gentile L, Stanley EF (2005) A unified model of presynaptic release site gating by calcium channel domains. Eur J Neurosci 21:278–282.

Glowatzki E, Fuchs PA (2002) Transmitter release at the hair cell ribbon synapse. Nat Neurosci 5:147–154.

Goutman JD, Glowatzki E (2007) Time course and calcium dependence of transmitter release at a single ribbon synapse. Proc Natl Acad Sci U S A 104:16341–16346.

Handrock R, Schröder F, Hirt S, Haverich A, Mittmann C, Herzig S (1998) Single-channel properties of L-type calcium channels from failing human ventricle. Cardiovasc Res 37:445–455.

He L, Xue L, Xu J, McNeil BD, Bai L, Melicoff E, Adachi R, Wu LG (2009) Compound vesicle fusion increases quantal size and potentiates synaptic transmission. Nature 459:93–97.

Heidelberger R, Heinemann C, Neher E, Matthews G (1994) Calcium dependence of the rate of exocytosis in a synaptic terminal. Nature 371:513–515.

Hering S, Sokolov S, Berjukow S, Marksteiner R, Margreiter E, Timin EN (2005) Calcium channel block and inactivation: insights from structure-activity studies. In: Voltage-gated calcium channels (Zamponi GW, ed), pp 281–293. London: Kluwer Academic/Plenum Publishers.

Hess P, Lansman JB, Tsien RW (1984) Different modes of Ca channel gating behaviour favoured by dihydropyridine Ca agonists and antagonists. Nature 311:538–544.

Isaacson JS, Walmsley B (1995) Counting quanta: direct measurements of transmitter release at a central synapse. Neuron 15:875–884.

Johnson SL, Marcotti W, Kros CJ (2005) Increase in efficiency and reduction in Ca2+ dependence of exocytosis during development of mouse inner hair cells. J Physiol 563:177–191.

Johnson SL, Franz C, Kuhn S, Furness DN, Rüttiger L, Münkner S, Rivolta MN, Seward EP, Herschman HR, Engel J, Knipper M, Marcotti W (2010) Synaptotagmin IV determines the linear Ca(2+) dependence of vesicle fusion at auditory ribbon synapses. Nat Neurosci 13:45–52.

Keen EC, Hudspeth AJ (2006) Transfer characteristics of the hair cell's afferent synapse. Proc Natl Acad Sci U S A 103:5537–5542.

Lacerda AE, Brown AM (1989) Nonmodal gating of cardiac calcium channels as revealed by dihydropyridines. J Gen Physiol 93:1243–1273.

Li GL, Keen E, Andor-Ardó D, Hudspeth AJ, von Gersdorff H (2009) The unitary event underlying multiquantal EPSCs at a hair cell's ribbon synapse. J Neurosci 29:7558–7568.

Liu L, Gonzalez PK, Barrett CF, Rittenhouse AR (2003) The calcium channel ligand FPL 64176 enhances L-type but inhibits N-type neuronal calcium currents. Neuropharmacology 45:281–292.

Llano I, González J, Caputo C, Lai FA, Blayney LM, Tan YP, Marty A (2000) Presynaptic calcium stores underlie large-amplitude miniature IPSCs and spontaneous calcium transients. Nat Neurosci 3:1256–1265.

Llinás R, Steinberg IZ, Walton K (1981) Relationship between presynaptic calcium current and postsynaptic potential in squid giant synapse. Biophys J 33:323–351.

Matthews G, Sterling P (2008) Evidence that vesicles undergo compound fusion on the synaptic ribbon. J Neurosci 28:5403–5411.

Morgan JL, Dhingra A, Vardi N, Wong RO (2006) Axons and dendrites originate from neuroepithelial-like processes of retinal bipolar cells. Nat Neurosci 9:85–92.

Neef A, Khimich D, Pirih P, Riedel D, Wolf F, Moser T (2007) Probing the mechanism of exocytosis at the hair cell ribbon synapse. J Neurosci 27:12933–12944.

Nowycky MC, Fox AP, Tsien RW (1985) Long-opening mode of gating of neuronal calcium channels and its promotion by the dihydropyridine calcium agonist Bay K 8644. Proc Natl Acad Sci U S A 82:2178–2182.

Palmer MJ, Hull C, Vigh J, von Gersdorff H (2003) Synaptic cleft acidification and modulation of short-term depression by exocytosed protons in retinal bipolar cells. J Neurosci 23:11332–11341.

Quastel DM, Guan YY, Saint DA (1992) The relation between transmitter release and Ca2+ entry at the mouse motor nerve terminal: role of stochastic factors causing heterogeneity. Neuroscience 51:657–671.

Raviola E, Raviola G (1982) Structure of the synaptic membranes in the inner plexiform layer of the retina: a freeze-fracture study in monkeys and rabbits. J Comp Neurol 209:233–248.

Rieke F, Lee A, Haeseleer F (2008) Characterization of Ca2+-binding protein 5 knockout mouse retina. Invest Ophthalmol Vis Sci 49:5126–5135.

Roberts WM, Jacobs RA, Hudspeth AJ (1990) Colocalization of ion channels involved in frequency selectivity and synaptic transmission at presynaptic active zones of hair cells. J Neurosci 10:3664–3684.

Schneggenburger R, Meyer AC, Neher E (1999) Released fraction and total size of a pool of immediately available transmitter quanta at a calyx synapse. Neuron 23:399–409.

Shahrezaei V, Cao A, Delaney KR (2006) Ca^{2+} from one or two channels controls fusion of a single vesicle at the frog neuromuscular junction. J Neurosci 26:13240–13249.

Sigworth FJ (1980) The variance of sodium current fluctuations at the node of Ranvier. J Physiol 307:97–129.

Silberberg SD, Magleby KL (1993) Preventing errors when estimating single channel properties from the analysis of current fluctuations. Biophys J 65:1570–1584.

Singer JH (2007) Multivesicular release and saturation of glutamatergic signalling at retinal ribbon synapses. J Physiol 580:23–29.

Singer JH, Diamond JS (2003) Sustained Ca^{2+} entry elicits transient postsynaptic currents at a retinal ribbon synapse. J Neurosci 23:10923–10933.

Singer JH, Diamond JS (2006) Vesicle depletion and synaptic depression at a mammalian ribbon synapse. J Neurophysiol 95:3191–3198.

Singer JH, Lassová L, Vardi N, Diamond JS (2004) Coordinated multivesicular release at a mammalian ribbon synapse. Nat Neurosci 7:826–833.

Snellman J, Zenisek D, Nawy S (2009) Switching between transient and sustained signalling at the rod bipolar-AII amacrine cell synapse of the mouse retina. J Physiol 587:2443–2455.

Stanley EF (1993) Single calcium channels and acetylcholine release at a presynaptic nerve terminal. Neuron 11:1007–1011.

Stanley EF (1997) The calcium channel and the organization of the presynaptic transmitter release face. Trends Neurosci 20:404–409.

Sterling P, Matthews G (2005) Structure and function of ribbon synapses. Trends Neurosci 28:20–29.

Suryanarayanan A, Slaughter MM (2006) Synaptic transmission mediated by internal calcium stores in rod photoreceptors. J Neurosci 26:1759–1766.

Tavalin SJ, Shepherd D, Cloues RK, Bowden SE, Marrion NV (2004) Modulation of single channels underlying hippocampal L-type current enhancement by agonists depends on the permeant ion. J Neurophysiol 92:824–837.

Thoreson WB, Rabl K, Townes-Anderson E, Heidelberger R (2004) A highly Ca2+-sensitive pool of vesicles contributes to linearity at the rod photoreceptor ribbon synapse. Neuron 42:595–605.

Tsukamoto Y, Morigiwa K, Ueda M, Sterling P (2001) Microcircuits for night vision in mouse retina. J Neurosci 21:8616–8623.

von Gersdorff H, Matthews G (1997) Depletion and replenishment of vesicle pools at a ribbon-type synaptic terminal. J Neurosci 17:1919–1927.

von Gersdorff H, Sakaba T, Berglund K, Tachibana M (1998) Submillisecond kinetics of glutamate release from a sensory synapse. Neuron 21:1177–1188.

Yoshikami D, Bagabaldo Z, Olivera BM (1989) The inhibitory effects of omega-conotoxins on Ca channels and synapses. Ann N Y Acad Sci 560:230–248.

Zhou ZY, Wan QF, Thakur P, Heidelberger R (2006) Capacitance measurements in the mouse rod bipolar cell identify a pool of releasable synaptic vesicles. J Neurophysiol 96:2539–2548.